ADVANCED MATERIALS
www.advmat.de

Check for updates

Photolithographic Patterning of Organic Color-Centers

*Zhongjie Huang, Lyndsey R. Powell, Xiaojian Wu, Mijin Kim, Haoran Qu, Peng Wang, Jacob L. Fortner, Beibei Xu, Allen L. Ng, and YuHuang Wang**

Organic color-centers (OCCs) have emerged as promising single-photon emitters for solid-state quantum technologies, chemically specific sensing, and near-infrared bioimaging. However, these quantum light sources are currently synthesized in bulk solution, lacking the spatial control required for on-chip integration. The ability to pattern OCCs on solid substrates with high spatial precision and molecularly defined structure is essential to interface electronics and advance their quantum applications. Herein, a lithographic generation of OCCs on solid-state semiconducting single-walled carbon nanotube films at spatially defined locations is presented. By using light-driven diazoether chemistry, it is possible to directly pattern *p*-nitroaryl OCCs, which demonstrate chemically specific spectral signatures at programmed positions as confirmed by Raman mapping and hyperspectral photoluminescence imaging. This light-driven technique enables the fabrication of OCC arrays on solid films that fluoresce in the shortwave infrared and presents an important step toward the direct writing of quantum emitters and other functionalities at the molecular level.

Quantum emitters (QEs), which generate photons one at a time, are the central building units of quantum technology.[1] The deterministic placement of solid-state QEs is essential to the construction and fabrication of on-chip photonic circuits and quantum networks in a scalable manner. However, many QEs are found as defects in crystal lattices, whose formation is inherently random and difficult to control.[2] Recently, there have been increasing efforts to create quantum emitting sites at defined locations in 2D materials, such as transition metal dichalcogenides[3] and hexagonal boron nitride.[4] However, these quantum emitting sites suffer from one or more of the following limitations, including low single photon purity, cryogenic operation, and ambiguous physical/chemical structures, making their optical properties difficult to control.[2d,3d,5]

Dr. Z. Huang, Dr. L. R. Powell, Dr. X. Wu, Dr. M. Kim, H. Qu, P. Wang, J. L. Fortner, Dr. B. Xu, Dr. A. L. Ng, Prof. Y. H. Wang
Department of Chemistry and Biochemistry
University of Maryland
College Park, MD 20742, USA
E-mail: yhw@umd.edu
Prof. Y. H. Wang
Maryland NanoCenter
University of Maryland
College Park, MD 20742, USA
The ORCID identification number(s) for the author(s) of this article can be found under https://doi.org/10.1002/adma.201906517.

DOI: 10.1002/adma.201906517

Organic color-centers (OCCs) are an emergent class of QEs that are synthesized by covalently bonding specific organic molecules on a host crystal substrate in a chemically controlled manner. The resulting OCCs serve as molecular focal points that can couple electrons, excitons, phonons, and spin to generate new material properties.[6] For example, sp^3 OCCs implanted into the sp^2 lattice of semiconducting single-walled carbon nanotubes (SWCNTs) produce quantum wells that can localize excitons,[7] brighten dark excitons,[8] and emit light as single photons with high purity at room temperature,[9] with the potential for applications in bioimaging,[10] chemical sensing,[11] telecommunications,[12] and quantum engineering.[9a–c] It has been demonstrated that the photoluminescent (PL) quantum yield of excitons confined in sp^3 OCCs can be at least one order of magnitude higher than that of the intrinsic band edge excitons of SWCNTs (typically ≈1% quantum yield).[13] Additionally, the emission wavelength of OCCs on SWCNTs can be systematically tuned by bonding different organic molecules to the surface and varying the chirality of the nanotube host to achieve telecom wavelengths for on-demand quantum communications.[14] However, the synthesis of OCCs to date has only been demonstrated in aqueous[8a,14,15] or organic[16] solutions of SWCNTs, but not yet on solid-state films, nor with spatial accuracy, which are required for many applications in optoelectronic devices, photonic systems, and quantum networks.

To address this challenge, in this work we demonstrate a direct-writing approach that enables us to fabricate patterns of OCCs on solid SWCNT films via a spatially resolved light-driven chemical reaction, as illustrated in **Figure 1**. To accomplish this, we deposited the *E*-isomer of *p*-nitrobenzenediazoascorbic acid (DZE) on the thin film and used light to drive localized reactions with SWCNTs that create the OCCs. Notably, the DZE is inert under dark conditions at room temperature (the *E*-isomer is the thermodynamically stable conformation) but can be switched to the highly-reactive *Z*-isomer when the SWCNT substrate is irradiated, according to our previous studies.[15a,b] With this chemistry, we show that programmed patterns of aryl functional groups can be directly written on a SWCNT thin film with light focused through the objective of a confocal microscope. Furthermore, we demonstrate that the molecular writing creates light-emitting OCC patterns that can be directly resolved with near-infrared PL hyperspectral imaging.

 © 2020 WILEY-VCH Verlag GmbH & Co. KGaA, Weinheim

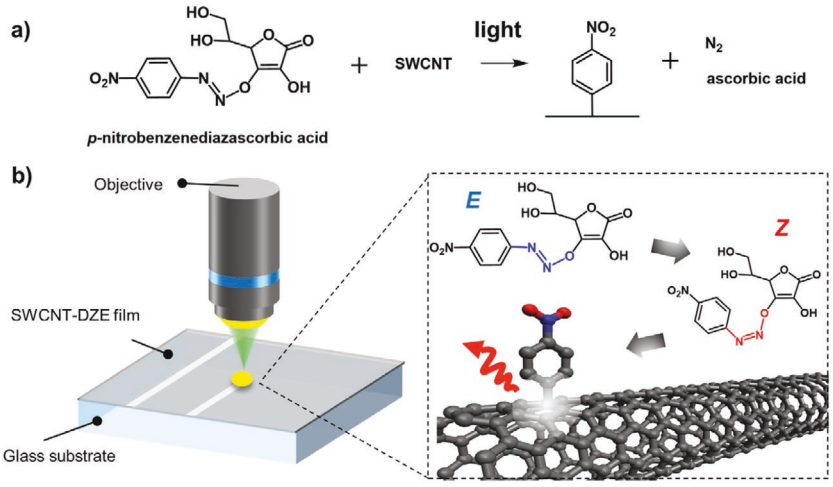

Figure 1. Photolithographic patterning of OCCs. a) The chemical equation of the light-directed reaction of *p*-nitrobenzenediazoascorbic acid on the SWCNT surface. Note that an OCC contains a pair of sp^3 defects, but for simplicity the 2nd group (H or OH) is omitted from the schemes. b) Scheme showing the spatially resolved OCC writing process. Exciting the SWCNT hosts with light drives local chemical reactions that create nitroaryl OCCs on the nanotube surfaces. By controlling the location of the light, we are able to fabricate patterns of OCCs that fluoresce in the shortwave infrared.

These findings pave the way for patterning of QEs and other functionalities at the molecular level.

As a first step, we formed a (6,5)-SWCNT-enriched thin film that featured a submonolayer of randomly interconnected nanotubes (**Figure 2**a) and used Raman spectroscopy to monitor the functionalization of the SWCNT thin film with *p*-nitroaryl groups via the light-activated DZE chemistry. Raman spectroscopy is useful for characterizing and monitoring the functionalization reaction degree, as the characteristic D- (≈1300 cm^{-1}) and G-bands (≈1590 cm^{-1}) of the SWCNTs arise from disordered structures in the sp^2 carbon (i.e., sp^3 carbon atoms) and the stretching of graphitic C—C bonds, respectively.[17] As a result, the ratio of these peaks (D/G) provides a powerful tool to examine the relative degree of sp^3 functionalization.[8a,18] The Raman laser was used for both "writing" (inducing covalent functionalization) and "reading" (detecting) the OCC functionalization sites. In the writing process,

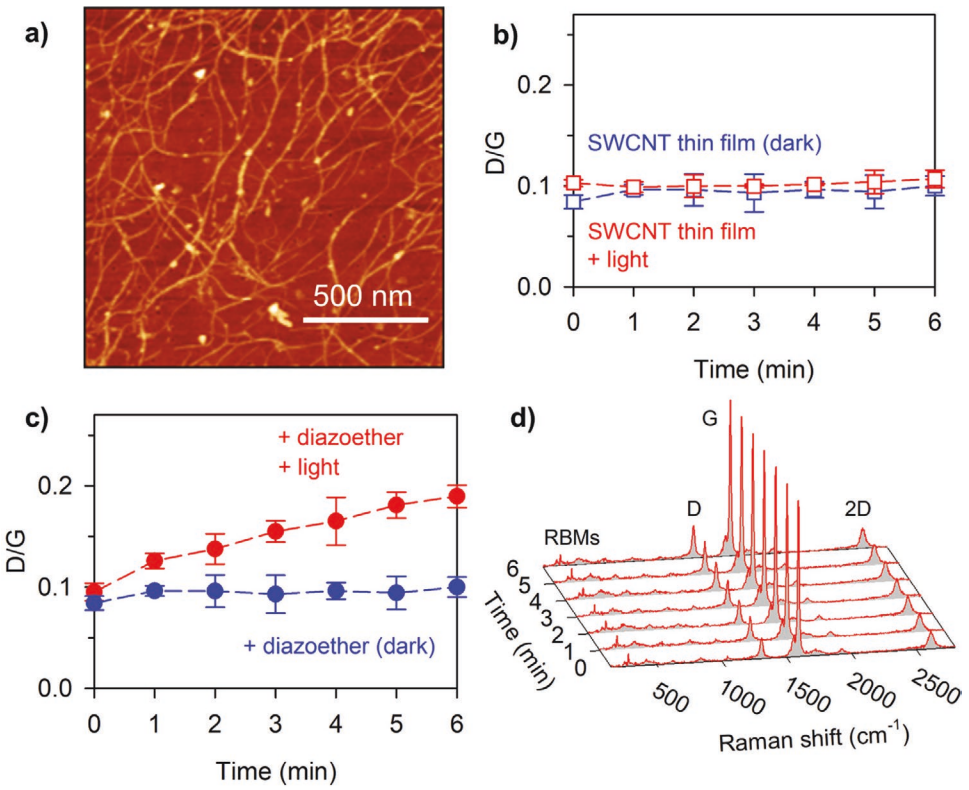

Figure 2. Raman characterization of *p*-nitroaryl OCC-functionalized SWCNT thin films. a) AFM image of a (6,5)-SWCNT thin film. b) Comparison of the D/G ratio of the SWCNT film in the absence of the diazoether reagent (*p*-nitrobenzenediazoascorbic acid) when irradiated (red) and kept in the dark (blue), in which little change in the D/G ratio is observed. Note that the SWCNT film has an inherent D peak due to native structural defects and impurities. c) Comparison of the D/G ratio of the SWCNT film in the presence of the diazoether irradiated by the 633 nm laser for up to 6 min (red) or kept in the dark (blue), in which the diazoether + light sample demonstrates a clear increase in the D/G ratio that corresponds to the spectra shown in (d). d) Raman spectra of the SWCNT film in the presence of the diazoether reagent revealing an increase in the D-peak with respect to the G-band upon irradiation (633 nm) for varying amounts of illumination time (0–6 min).

© 2020 WILEY-VCH Verlag GmbH & Co. KGaA, Weinheim

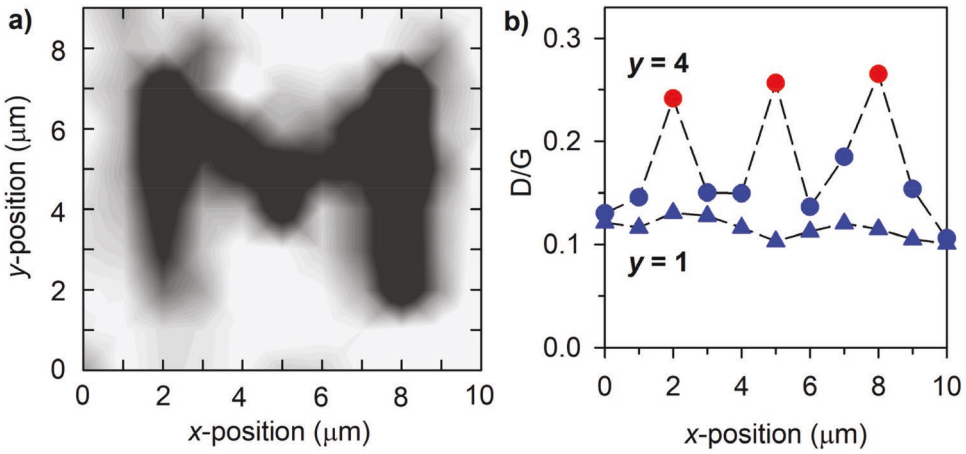

Figure 3. 2D patterning of *p*-nitroaryl OCCs on a SWCNT film. a) Contour plot of the D/G ratio at different locations on the SWCNT film patterned with nitroaryl groups in the shape of the letter "M." The darker regions indicate higher D/G ratios. b) The D/G ratio plotted along the length of $y = 4$ and $y = 1$ in (a). The red data points correspond to spots that were irradiated, while the blue data points correspond to areas that were not exposed to the laser.

the incident output of the HeNe laser (633 nm, 1.96 eV) was focused through a high-resolution objective (100×, 0.9 NA) to expose diffraction-limited regions (≈860 nm in diameter) of the film for increments of 1 min, for up to 6 min total. Then the sample was cooled for 1 min before the Raman spectrum of the sample was collected (i.e., the reading process, with 6 s exposure). Since laser-induced damage to the SWCNTs will also increase the D/G ratio, we first optimized the photon fluence of the laser to ensure that the functionalization reaction could be conducted without photodamaging the nanotube substrate. It should be noted that the SWCNT film has an inherent D peak due to native structural defects and impurities.[18c,19] We found that an irradiation power density of 1.4×10^5 W cm^{-2} at 633 nm did not induce a detectable increase of the D/G ratio in the SWCNT film alone, even after up to 6 min of irradiation (Figure 2b). We thus used this irradiation power density for all Raman experiments, in both the writing and reading processes.

We then deposited DZE on the SWCNT film and protected the sample from light. The relatively little change in the D/G ratio (read-only) indicated no functionalization reaction was detected (blue plot in Figure 2c). This observation agrees well with the inertness of the *E*-isomer of DZE in the dark.[15b] However, when the sample was irradiated by the 633 nm laser (which only excites the SWCNT, not DZE, see Figure S1, Supporting Information), the D/G ratio gradually increased with the irradiation time, nearly doubling, which indicates the successful creation of sp^3 defects and the grafting of *p*-nitroaryl molecules to the nanotube surfaces (red plot in Figure 2c, representative spectra shown in Figure 2d). In this work we targeted low defect densities of OCCs (to maximize the potential PL intensity),[6,15a] therefore we stopped monitoring the reaction prior to saturation of the D/G ratio.

We further show it is possible to apply this light-driven chemistry to directly write OCC patterns on the SWCNT substrate. As a demonstration, we used the mapping capabilities of the Raman microscope to pattern *p*-nitroaryl functional group arrays in an "M" shape on the SWCNT thin film. The "M" shaped design of the laser irradiation pattern is shown in Figure S2a, Supporting Information, in which the grey squares depict the irradiation spots in the serial writing process. We chose a step size of 1 μm to perform this patterning experiment. **Figure 3**a shows the scale of the Raman D/G ratio across the surface of the sample, in which the high D/G region forms the shape of an "M," which corresponds to the light-written pattern, indicating the effective grafting of the functional groups in these areas. Figure 3b shows the D/G ratios along the lines defined by $y = 1$ and $y = 4$ in the sample coordinates. At $y = 4$, the D/G ratio possesses distinct values at different x positions, depending on whether the area was included in the irradiation pattern of the writing process. For example, the spectra measured at the locations of $x = 2$, 5, and 8 display significantly higher D/G ratios compared to the other positions along this trace. As a comparison, the D/G ratio along $y = 1$ remains relatively low and constant, which is consistent with the irradiation pattern design. The feature size and pitch of these samples were at a 1 μm scale, which demonstrates the capability of the molecular writing at high resolution.

The covalent attachment of various functional groups on SWCNTs in aqueous solution can generate OCCs that display a new PL peak (E_{11}^-) that is distinct from the intrinsic emission of the SWCNT host (E_{11}) and characteristic of the electronic structure of the emitting center.[6,8a,14,15,20] However, it remains unclear whether this kind of light-driven chemistry can be realized on solid films to directly generate QE patterns featuring this characteristic E_{11}^- emission peak of OCCs. Therefore, as a proof-of-concept demonstration, we used the same light-activated DZE chemistry to write QE patterns on SWCNT thin films. It is worth noting that the required functional degree and detection sensitivity is quite different for Raman scattering measurements and PL imaging, in which the functional density must be fairly low in order to observe maximized E_{11}^- PL signal, compared to the higher amount needed to detect a Raman signal on conventional Raman microscopes.[6,15a] Therefore, the experimental conditions need to be adjusted for QE writing to achieve an appropriate functional degree and appreciable defect emission.

© 2020 WILEY-VCH Verlag GmbH & Co. KGaA, Weinheim

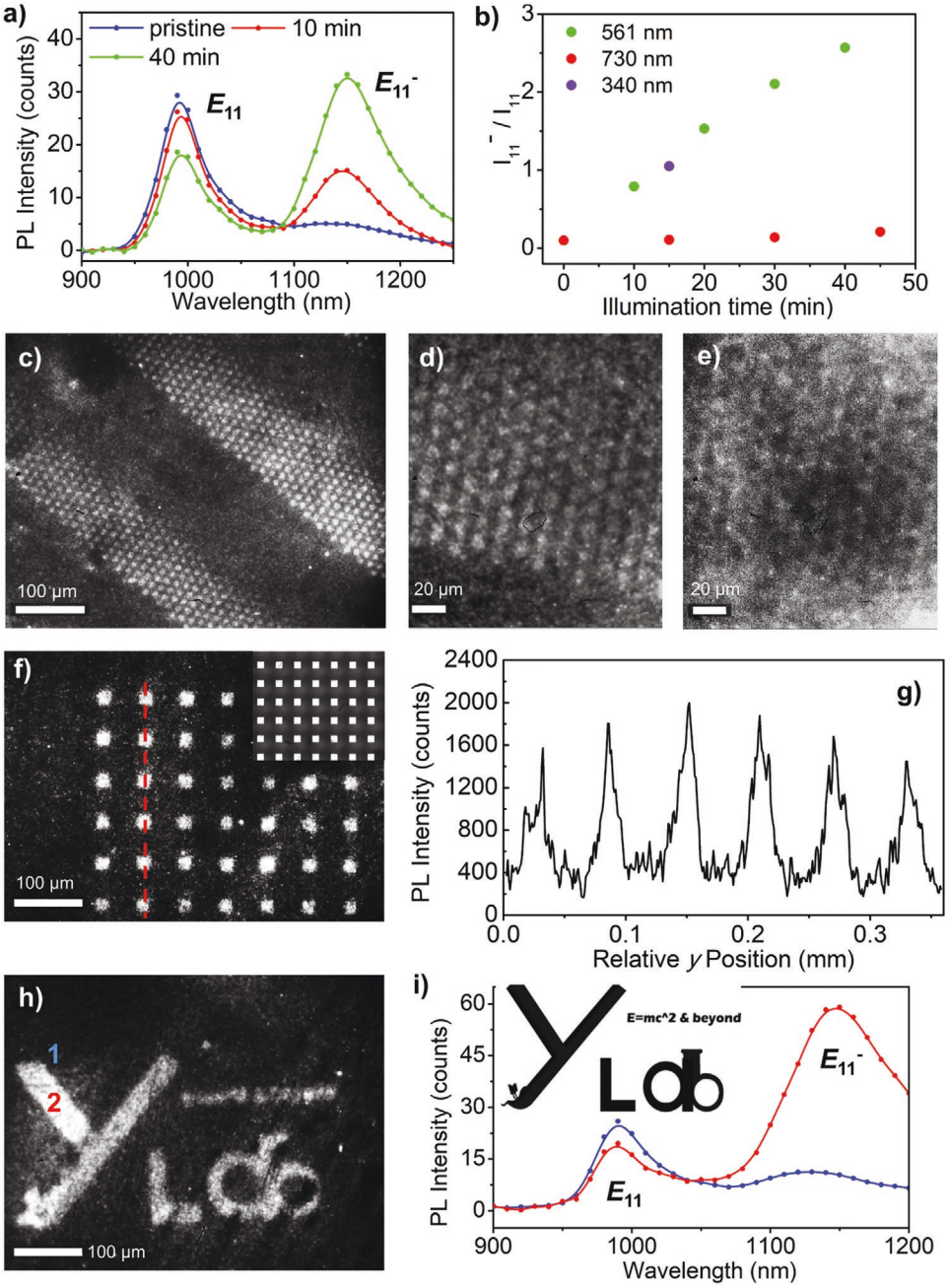

Figure 4. Light-directed functionalization generates patterns of NIR fluorescent OCCs on SWCNT films. a) PL spectra of the SWCNT-DZE film exposed to 561 nm irradiation with various illumination time. b) The effect of the illumination wavelength and time on the functionalization degree. c–e) PL images of the film after illumination by 340 nm light through a shadow mask with arrays of 8 μm microfabricated holes. Note that the PL images were collected with a 1100 nm long pass optical filter (c,d) and a 980 ± 10 nm band pass filter (e). f–i) PL images (collected with a 1100 nm long pass optical filter) of the film after illumination by 532 nm light in the DMD-assisted pattern, consisting of an array of 23 μm × 23 μm squares (f) at 60 μm pitches (the inset in the top right corner in (f) shows the optical microscopy image of the illumination pattern on the film, and the PL emission intensity profile along the red dashed line is shown in (g)); and a custom-designed "Y_{Lab}" logo ((h) and inset of (i)), with representative PL spectra of the regions of interest, labeled as "1" (blue) and "2" (red) in (h) on the film plotted in (i).

In our QE writing experiments, a SWCNT-DZE film was deposited on a glass slide by drop-casting a pre-mixed solution of (6,5)-SWCNTs and DZE. Then we illuminated the film to promote the formation of OCCs on the SWCNT surfaces (the "writing" process), and characterized the resulting material using a custom-built hyperspectral shortwave IR imaging system[15d,21] with an excitation light source of 730 nm (the "reading" process). Two typical approaches were utilized to characterize the functionalized SWCNT film, and the representative results are shown in **Figure 4**. The first approach involved

© 2020 WILEY-VCH Verlag GmbH & Co. KGaA, Weinheim

a hyperspectral fluorescence cube scan, which obtains the PL spectra of the sample for each pixel. The other was broadband imaging filtered by a 1100 nm long-pass filter, which was used to spectrally exclude the intrinsic E_{11} PL of the (6,5)-SWCNT itself (≈990 nm) from the OCC emission signal.

We investigated the effect of the illumination condition on the QE writing process on the solid SWCNT films. We first used a 561 nm laser (at a power density of 20 W cm^{-2}) on the hyperspectral microscope and a 20× objective (field of view ≈600 µm × 500 µm) to conduct the functionalization reaction. Note that this laser line resonates with the E_{22} transition band of (6,5)-SWCNT and thus requires a lower power density to trigger the reaction (compared with the 633 nm and 730 nm lasers). The averaged PL spectra of the film are shown in Figure 4a with different exposure times to the 561 nm laser during the writing process. Covalent bonding of the *p*-nitroaryl functional groups to the thin film is evidenced by the rise of the E_{11}^- emission feature at ≈1150 nm characteristic of the OCC.[15b] Additionally, the peak intensity increases with illumination time. These experiments suggest the successful covalent bonding of the *p*-nitroaryl functional groups, leading to the creation of OCCs on a thin film.

We used the E_{11}^- to E_{11} PL ratio (noted as I_{11}^-/I_{11}, obtained by integration of the peak areas) to further evaluate the areal density of OCCs at different illumination conditions applied in the writing process, as shown in Figure 4b. At the same illumination intensity (20 W cm^{-2}), the functional degree increases rapidly with 561 nm illumination, but very slowly when using 730 nm wavelength illumination, which is not directly resonant with the optical transitions of (6,5)-SWCNTs (i.e., E_{11}, E_{22}, E_{33}...), but only with the broad carbon absorption. Furthermore, the functionalization can be achieved using 340 nm UV irradiation (at an even weaker power density, 0.08 W cm^{-2}), which resonates with the E_{33} transition band of (6,5)-SWCNTs and can directly excite the *E*-isomer of DZE. Figure 4b reveals that excitation in resonance with the absorption features of SWCNTs can promote the reaction. We also investigated the effect of different illumination conditions and DZE concentration on the QE writing, as summarized in Table S1, Supporting Information. In particular, the same illumination condition as reported for the liquid phase reaction (561 nm, 0.0115 W cm^{-2})[15b] can trigger the functionalization on the solid film, though at a much slower rate (I_{11}^-/I_{11} only reached ≈0.2 after 8 h of illumination).

For a simple demonstration of QE patterning, we covered the solid film with a mask (Figure S3, Supporting Information) featuring parallel arrays of holes (8 µm diameter pores, with a pitch of 13 µm), through which the sample was illuminated by 340 nm light for 15 min. Figure 4c shows the resulting arrays of OCC dots, whose pattern resembles that of the mask. The PL images of the same film under a 50× objective filtered by a 1100 nm long-pass filter (only photons emitted at wavelengths greater than 1100 nm were recorded, allowing the E_{11}^- emission to be exclusively imaged) and a band-pass filter (which only collects light with wavelength of 980 ± 10 nm, corresponding to the E_{11} emission) are displayed for comparison in Figure 4d,e, respectively. Besides the clear OCC pattern resulting from the E_{11}^- emission (Figure 4d), a very weak pattern of the intrinsic E_{11} SWCNT emission (Figure 4e) can be observed as well, thus demonstrating a small partial loss of the E_{11} intensity at the OCC functionalized sites, as also revealed in Figure 4a. These experiments directly show that the QE patterns were successfully created by our spatially resolved light-driven chemistry in the OCC writing process.

We further demonstrated that custom designed patterns can be realized through mask-free techniques. We utilized a digital micromirror device (DMD) coupled with a TERA-Fab E series printer (Figure S4, Supporting Information), on which arrays of micromirrors and the on/off state (reflecting or blocking light) of each micromirror can be independently controlled to project visible LED light (532 nm in wavelength, ≈0.5 W cm^{-2}) to selected areas on the substrate through a microscope objective (20×, 0.42 NA). For this type of parallel writing process, we designed a periodic square array pattern (23 µm × 23 µm for each square, 60 µm pitch) and illuminated the SWCNT-DZE film for 3 h. Figure 4f shows the long-pass filtered PL image of the film after patterning. The resulting QE arrays closely resemble the illumination pattern on the film (optical microscopy image shown in the inset of Figure 4f). The PL intensity for the areas along the red dashed line marked in Figure 4f is shown in Figure 4g, in which the periodic intensity of the signal possesses a period of ≈60 µm, which is consistent with the pitch of the illumination pattern.

As another demonstration of writing these QEs in an arbitrary form, we printed a custom-designed "Y_{Lab}" logo (inset of Figure 4i) on the solid SWCNT film (Figure 4h). The PL spectra of representative non-illuminated (labeled as "1" in Figure 4h) and illuminated (labeled as "2") regions of the film are compared in Figure 4i. It should be noted that the E_{11}^- peak position (≈1150 nm) was constant for all the *p*-nitroaryl OCCs created in this work and agrees well with that of the same type of OCC synthesized in aqueous solution.[8a,15a,b] Therefore, our OCCs arise unambiguously from the bonding of *p*-nitroaryl groups on the SWCNTs, not by other side reactions such as doping of oxygen, which is known to typically emit at 1120 nm for (6,5)-SWCNTs.[22] Note that the OCC patterns are stable at ambient conditions. Even after 104 days of storage in a Petri dish placed on a lab shelf without specific light protection or removing the unreacted *E*-isomers from the surface, the fabricated OCC patterns remain clearly presented as shown in Figure S5, Supporting Information.

Our study unambiguously demonstrates the successful spatially-resolved bonding of functional moieties on solid SWCNT substrates and the creation of OCC patterns, paving the way for integrating OCCs with conventional photolithography protocols. Currently, the resolution of the patterning observed by hyperspectral imaging is limited to a few microns, which is slightly larger than that of the molecular writing resolved by Raman scattering. This difference in feature size is due to the different functional degrees we targeted, as well as the different detection sensitivities and illumination conditions of each platform. In particular, the PL intensity of each SWCNT can be affected by other factors, including the nanotube length,[7b,21a] areal density, surfactant wrapping,[22b,23] surface adsorption,[24] and local environment.[25] Further improvement of the thin film quality (nanotube packing, chirality purity, and film uniformity), and localized delivery of the reactants (e.g., through microcontact printing[26] or scanning probe lithography[27])

© 2020 WILEY-VCH Verlag GmbH & Co. KGaA, Weinheim

and/or the light[28] that triggers the reaction should make it possible to increase the patterning resolution further.

In addition, our approach is not limited to DZE chemistry and nitroaryl functional groups, but could be expanded and applied to a wide class of OCCs with light-driven reaction mechanisms.[6,8a,14,15] In general, the molecular tunability of OCCs provides an opportunity to constructively functionalize the host in a controllable manner, in which a variety of different molecular groups can bond to the host surface.[14] The ability to drive many of these reactions by exciting the substrate with light offers unique opportunities to leverage the near-field light delivery capabilities of beam pen lithography.[28,29] With further improvement of the chemistry kinetics, SWCNT film quality, and the potential inclusion of a microfluidic system to deposit different molecules on the same SWCNT substrate,[30] it should be possible to create spatially correlated, high-resolution molecular patterns and a diverse array of functional moieties to form a multi-functional molecular platform for advanced applications (e.g., multiplexing sensing).

In conclusion, we present a scalable fabrication of OCC patterns on solid films via light-directed bonding of molecular functional groups. We have successfully developed this method to expand the functionality of SWCNT films by synthetically creating few-µm scale patterns of near-IR QEs on the surface of the substrate. With further development of our technique, along with progress in detecting single defects,[21c,31] we expect that the resolution of this OCC writing process could reach the single functional group level. This would open opportunities for in-depth studies of OCC chemistry and physics at the single molecule level and the interaction between neighboring defects via the coupling of electrons, excitons, phonons, and spin, as well as making practical applications possible, such as single photon sources.[6] Furthermore, we envision applying our approach to constructively modify other material hosts beyond carbon nanotubes (such as 2D transition metal dichalcogenides)[32] with high chemical and spatial precision.

Experimental Section

Preparation of Chirality-Enriched SWCNT Thin Films: HiPco materials (batch no. 194.3, Rice University) were suspended by 1 wt% sodium dodecyl sulfate (SDS, 99%, Sigma-Aldrich) in Nanopure water (18 MΩ) by ultrasonication (Misonix, 1/2 inch flat tip, 4 h in pulsed mode [10 s on and 2 s off, 36 W]). Impurities and bundles were separated from the surfactant-suspended nanotubes by ultracentrifugation using an Optima XE-90 ultracentrifuge (Beckman Coulter, SW41 Ti rotor, 30000 × *g*)[33] and decanting the top fraction for further processing. The (6,5)-SWCNTs were then separated from the heterogeneous suspension of metallic and semiconducting SWCNTs by a multicolumn gel chromatography procedure using columns of Sephacryl S-200 HR (GE Healthcare) with a method adapted from Liu et al.[34]

Thin films of (6,5)-SWCNTs on glass substrates for Raman characterization were fabricated using a previously described method by Ng et al.,[35] in which a solution of (6,5)-SWCNTs was filtered over a nitrocellulose membrane (25 nm pore size; Millipore VSWP). The film density was calculated based on the concentration of the (6,5)-SWCNT solution (determined by its optical absorbance at E_{11}).[36] The film was washed with copious amounts of Nanopure water to remove surfactants and impurities and dried in vacuum at room temperature for 12 h. The film was cut and a ≈1 cm^2 portion was transferred to a quartz slide by a thermal transfer method[21b,37] and the nitrocellulose membrane was removed using an acetone vapor bath (105 °C for 72 h) and subsequent incubation in acetone (60 °C for 4 h). The SWNCT film on the quartz substrate was immersed in Nanopure water for 2 h before being dried in vacuum (24 h). For control experiments, the film was used directly from the vacuum oven. In the case of experiments with DZE functionalization, the protocol below was followed.

Application of p-Nitrobenzenediazoascorbic Acid to SWCNT Films for Raman Spectroscopy: *p*-Nitrobenzenediazoascorbic acid was prepared according to a previously reported method,[15b] and its absorption spectrum (Figure S1, Supporting Information) indicates its *E*-isomer state under ambient conditions. A drop (≈40 µL) of a 50 µM aqueous solution of the *p*-nitrobenzenediazoascorbic acid was carefully drop-cast to cover the SWCNT film in a Petri dish. The Petri dish was covered in aluminum foil and the film was incubated at room temperature for 30 min in the dark to allow sufficient time for the diazoether to adsorb to the SWCNT film surface. After 30 min, the remaining diazoether solution was carefully removed by pipette and the film was dried for 30 min at room temperature with protection from light.

Irradiation and Characterization of the Patterned SWCNT Film by Resonant Raman Spectroscopy: A Raman laser in a confocal microscope (Horiba Jobin-Yvon LabRam ARAMIS) was used for both inducing functionalization (increments of 1 min irradiation) in the writing process and monitoring the reaction (6 s measurement dwell time) in the reading process. The incident 633 nm laser light was focused through a high-resolution 100× objective (0.9 NA, Olympus) to resolve µm-scale regions of the film. Each experiment was performed on three different spots on the sample film, and the averaged D/G ratio was presented in this work. A power density of ≈1.4×10^5 W cm^{-2} was used for all our writing and reading experiments. For the 2D patterning experiment, selective areas of the DZE-covered SWCNT film (see Figure S2a, Supporting Information) were irradiated for serial writing, and the resulting film was characterized by 2D Raman mapping.

Irradiation and Characterization of Near-Infrared Photoluminescence by Hyperspectral Imaging: The SWCNT-DZE film for PL measurement was prepared by drop-casting a pre-mixed solution of 2 µL of (6,5)-SWCNT (≈150 µM of carbon in 1 wt% SDS) and 4 µL of 50 µM DZE on a glass substrate (Thermo Scientific, NH), and allowed to completely dry in the dark. Note that the dried film contains a flat area of ≈7 mm^2 in the middle, which is sufficiently large for this experiment. The film has a thickness of ≈200 nm, as measured by a profilometer (Tencor Alpha Step 200), and contains the nanotubes embedded in SDS.

In the patterning experiment with a shadow mask, the SWCNT-DZE film sample was covered by a mask (Figure S3, Supporting Information) containing parallel arrays of holes (8 µm diameter pores, with a pitch of 13 µm) and exposed to 340 nm LED light source (M340L4, Thorlabs, NJ) with an intensity of 0.08 W cm^{-2} for 15 min. The Si_3N_4 membrane (Aquamarijn, Netherlands) was coated by 100 nm of Au through thermal deposition (to improve the transmission contrast) and used as the shadow mask for this experiment.

In the mask-free patterning experiments, a DMD coupled TERA-Fab E series printer (Tera-print, IL, see Figure S4, Supporting Information) was used to project visible LED light (532 nm in wavelength) to selected areas through a 20× microscope objective (Mitutoyo, 0.42 NA) with an optical power intensity of 0.5 W cm^{-2}. The DMD contains square arrays of micromirrors, and the on/off state of each micromirror can be independently programmed to either reflect or block the passing light. As a result, unique illumination patterns can be created through the instrument's software (TERA-print, LLC; Tera-e version 1.6). The patterns used in this work were a periodic array of squares (each square was 23 µm × 23 µm, at 60 µm pitch) and a custom-designed "Y_{Lab}" logo. The illumination time for each sample was 3 h.

We used a custom-built hyperspectral shortwave near-IR imaging system[21c] to characterize the patterned OCCs and to in situ investigate the effect of some of the illumination conditions. The experiments were performed on a Nikon Eclipse U inverted microscope with IR-optimized objectives (Olympus LCPLN20XIR, 0.45 NA, or LCPLN50XIR, 0.65 NA), a 730 nm (Shanghai Dream Lasers Technology Co., Ltd.) and a 561 nm laser source (Jive Cobolt AB, Sweden). The fluorescence, excited by the

© 2020 WILEY-VCH Verlag GmbH & Co. KGaA, Weinheim

730 nm laser, was detected using a 640 × 512 pixel InGaAs focal plane array (Cougar-640, Xenics; Belgium) cooled to –190 °C. PL spectra were reconstructed from hyperspectral fluorescence cube scans from 900 to 1250 nm wavelengths with 10 nm intervals. In addition, to exclusively image the OCC sites, a 1100 nm long pass filter (Thorlabs, FELH1100) was used to isolate the OCC emission (≈1150 nm) from that of the (6,5)-SWCNT (≈990 nm). Note that the background signal of the glass substrate was subtracted from the PL data shown in this work. For the in situ generation and characterization of OCCs, the 561 nm and 730 nm lasers (with an intensity adjusted to 20 W cm^{-2}) were used to induce the OCC generation on solid films through a 20× objective of the hyperspectral microscope and imaged using the 730 nm laser as the excitation source.

UV–vis–NIR Absorption Spectroscopy: The absorption spectra (1 cm path length) of the (6,5)-SWCNT and DZE solutions were measured using a PerkinElmer Lambda 1050 UV–vis–NIR spectrophotometer.

Atomic Force Microscopy: The atomic force microscopy (AFM) image was recorded in tapping mode on a Cypher ES AFM (Asylum Research Corporation, CA) with conical AFM probes backside-coated with gold (Tap300GD-G, with a force constant of 40 N m^{-1}, Ted Pella).

Supporting Information

Supporting Information is available from the Wiley Online Library or from the author.

Acknowledgements

Z.H., L.R.P., and X.W. contributed equally to this work. This work was partially supported by the Air Force Office of Scientific Research award (Multidisciplinary University Research Initiatives FA9550-16-1-0150), which made it possible to develop the patterning tool, and the National Science Foundation (grant no. CHE1904488), which supported the synthesis of the OCCs. The authors also gratefully acknowledge the National Science Foundation Major Research Instrumentation program (CHE1626288) for supporting a shared AFM system that was used to perform the AFM measurements. They also thank J. Magoline and A. Ivankin for help on the Tera-Fab instruments. L.R.P. gratefully acknowledges the Millard Alexander Fellowship in Chemistry.

Conflict of Interest

The authors declare no conflict of interest.

Keywords

carbon nanotubes, organic color-centers, photoluminescence, quantum emitters, Raman spectroscopy

Received: October 4, 2019
Revised: January 16, 2020
Published online:

[1] J. L. O'Brien, A. Furusawa, J. Vuckovic, *Nat. Photonics* **2009**, *3*, 687.
[2] a) Y. M. He, G. Clark, J. R. Schaibley, Y. He, M. C. Chen, Y. J. Wei, X. Ding, Q. Zhang, W. Yao, X. D. Xu, C. Y. Lu, J. W. Pan, *Nat. Nanotechnol.* **2015**, *10*, 497; b) C. Chakraborty, L. Kinnischtzke, K. M. Goodfellow, R. Beams, A. N. Vamivakas, *Nat. Nanotechnol.* **2015**, *10*, 507; c) M. Koperski, K. Nogajewski, A. Arora, V. Cherkez, P. Mallet, J. Y. Veuillen, J. Marcus, P. Kossacki, M. Potemski, *Nat. Nanotechnol.* **2015**, *10*, 503; d) I. Aharonovich, D. Englund, M. Toth, *Nat. Photonics* **2016**, *10*, 631.
[3] a) A. Branny, S. Kumar, R. Proux, B. D. Gerardot, *Nat. Commun.* **2017**, *8*, 15053; b) C. Palacios-Berraquero, D. M. Kara, A. R. P. Montblanch, M. Barbone, P. Latawiec, D. Yoon, A. K. Ott, M. Loncar, A. C. Ferrari, M. Atature, *Nat. Commun.* **2017**, *8*, 15093; c) Y. Luo, G. D. Shepard, J. V. Ardelean, D. A. Rhodes, B. Kim, K. Barmak, J. C. Hone, S. Strauf, *Nat. Nanotechnol.* **2018**, *13*, 1137; d) M. R. Rosenberger, C. K. Dass, H. J. Chuang, S. V. Sivaram, K. M. McCreary, J. R. Hendrickson, B. T. Jonker, *ACS Nano* **2019**, *13*, 904; e) S. Kumar, A. Kaczmarczyk, B. D. Gerardot, *Nano Lett.* **2015**, *15*, 7567.
[4] J. Ziegler, R. Klaiss, A. Blaikie, D. Miller, V. R. Horowitz, B. J. Aleman, *Nano Lett.* **2019**, *19*, 2121.
[5] B. Heinrich, *Nat. Nanotechnol.* **2019**, *14*, 100.
[6] A. H. Brozena, M. Kim, L. R. Powell, Y. Wang, *Nat. Rev. Chem.* **2019**, *3*, 375.
[7] a) N. F. Hartmann, S. E. Yalcin, L. Adamska, E. H. Haroz, X. D. Ma, S. Tretiak, H. Htoon, S. K. Doorn, *Nanoscale* **2015**, *7*, 20521; b) N. Danne, M. Kim, A. G. Godin, H. Kwon, Z. H. Gao, X. J. Wu, N. F. Hartmann, S. K. Doorn, B. Lounis, Y. H. Wang, L. Cognet, *ACS Nano* **2018**, *12*, 6059.
[8] a) Y. M. Piao, B. Meany, L. R. Powell, N. Valley, H. Kwon, G. C. Schatz, Y. H. Wang, *Nat. Chem.* **2013**, *5*, 840; b) Q. H. Wang, M. S. Strano, *Nat. Chem.* **2013**, *5*, 812.
[9] a) X. W. He, N. F. Hartmann, X. D. Ma, Y. Kim, R. Ihly, J. L. Blackburn, W. L. Gao, J. Kono, Y. Yomogida, A. Hirano, T. Tanaka, H. Kataura, H. Htoon, S. K. Doorn, *Nat. Photonics* **2017**, *11*, 577; b) K. Srinivasan, M. Zheng, *Nat. Photonics* **2017**, *11*, 535; c) A. Ishii, X. W. He, N. F. Hartmann, H. Machiya, H. Htoon, S. K. Doorn, Y. K. Kato, *Nano Lett.* **2018**, *18*, 3873; d) M. Nutz, J. Zhang, M. Kim, H. Kwon, X. Wu, Y. Wang, A. Högele, *Nano Lett.* **2019**, *19*, 7078.
[10] a) G. S. Hong, S. O. Diao, A. L. Antaris, H. J. Dai, *Chem. Rev.* **2015**, *115*, 10816; b) A. G. Godin, J. A. Varela, Z. H. Gao, N. Danne, J. P. Dupuis, B. Lounis, L. Groc, L. Cognet, *Nat. Nanotechnol.* **2017**, *12*, 238; c) J. A. Varela, J. P. Dupuis, L. Etchepare, A. Espana, L. Cognet, L. Groc, *Nat. Commun.* **2016**, *7*, 10947.
[11] a) H. Kwon, M. Kim, B. Meany, Y. M. Piao, L. R. Powell, Y. H. Wang, *J. Phys. Chem. C* **2015**, *119*, 3733; b) T. Shiraki, H. Onitsuka, T. Shiraishi, N. Nakashima, *Chem. Commun.* **2016**, *52*, 12972.
[12] N. Gisin, R. Thew, *Nat. Photonics* **2007**, *1*, 165.
[13] X. W. He, L. Y. Sun, B. J. Gifford, S. Tretiak, A. Piryatinski, X. Q. Li, H. Htoon, S. K. Doorn, *Nanoscale* **2019**, *11*, 9125.
[14] H. Kwon, M. Furmanchuk, M. Kim, B. Meany, Y. Guo, G. C. Schatz, Y. H. Wang, *J. Am. Chem. Soc.* **2016**, *138*, 6878.
[15] a) L. R. Powell, Y. M. Piao, Y. H. Wang, *J. Phys. Chem. Lett.* **2016**, *7*, 3690; b) L. R. Powell, M. Kim, Y. H. Wang, *J. Am. Chem. Soc.* **2017**, *139*, 12533; c) X. J. Wu, M. Kim, H. Kwon, Y. H. Wang, *Angew. Chem., Int. Ed.* **2018**, *57*, 648; d) H. Luo, P. Wang, X. Wu, H. Qu, X. Ren, Y. Wang, *ACS Nano* **2019**, *13*, 8417.
[16] F. J. Berger, J. Lüttgens, T. Nowack, T. Kutsch, S. Lindenthal, L. Kistner, C. C. Müller, L. M. Bongartz, V. A. Lumsargis, Y. Zakharko, J. Zaumseil, *ACS Nano* **2019**, *13*, 9259.
[17] a) M. S. Dresselhaus, G. Dresselhaus, R. Saito, A. Jorio, *Phys. Rep.* **2005**, *409*, 47; b) S. Costa, E. Borowiak-Palen, M. Kruszynska, A. Bachmatiuk, R. J. Kalenczuk, *Mater. Sci. (Poland)* **2008**, *26*, 433; c) T. Hummer, J. Noe, M. S. Hofmann, T. W. Hansch, A. Hogele, D. Hunger, *Nat. Commun.* **2016**, *7*, 12155.
[18] a) S. L. Deng, Y. Zhang, A. H. Brozena, M. L. Mayes, P. Banerjee, W. A. Chiou, G. W. Rubloff, G. C. Schatz, Y. H. Wang, *Nat. Commun.* **2011**, *2*, 382; b) M. Kim, L. Adamska, N. F. Hartmann, H. Kwon, J. Liu, K. A. Velizhanin, Y. M. Piao, L. R. Powell, B. Meany, S. K. Doorn, S. Tretiak, Y. H. Wang, *J. Phys. Chem. C* **2016**, *120*,

 © 2020 WILEY-VCH Verlag GmbH & Co. KGaA, Weinheim

11268; c) F. Gardea, Z. J. Huang, B. Glaz, S. P. Karna, X. Y. Cheng, Z. W. Peng, Y. H. Wang, *Adv. Mater. Interfaces* **2018**, *5*, 1800038.
[19] W. Z. Qian, T. Liu, F. Wei, Z. W. Wang, G. H. Luo, H. Yu, Z. F. Li, *Carbon* **2003**, *41*, 2613.
[20] M. Kim, X. J. Wu, G. Y. Ao, X. W. He, H. Kwon, N. F. Hartmann, M. Zheng, S. K. Doorn, Y. H. Wang, *Chem* **2018**, *4*, 2180.
[21] a) Y. Li, X. Wu, M. Kim, J. Fortner, H. Qu, Y. Wang, *Chem. Mater.* **2019**, *31*, 4536; b) P. Wang, M. J. Kim, Z. W. Peng, C. F. Sun, J. Mok, A. Lieberman, Y. H. Wang, *ACS Nano* **2017**, *11*, 9231; c) X. Wu, M. Kim, H. Qu, Y. Wang, *Nat. Commun.* **2019**, *10*, 2672.
[22] a) S. Ghosh, S. M. Bachilo, R. A. Simonette, K. M. Beckingham, R. B. Weisman, *Science* **2010**, *330*, 1656; b) C. F. Chiu, W. A. Saidi, V. E. Kagan, A. Star, *J. Am. Chem. Soc.* **2017**, *139*, 4859.
[23] L. J. Li, R. J. Nicholas, C. Y. Chen, R. C. Darton, S. C. Baker, *Nanotechnology* **2005**, *16*, S202.
[24] a) T. Uda, A. Ishii, Y. K. Kato, *ACS Photonics* **2018**, *5*, 559; b) C. Georgi, N. Hartmann, T. Gokus, A. A. Green, M. C. Hersam, A. Hartschuh, *ChemPhysChem* **2008**, *9*, 1460.
[25] a) X. J. Liu, H. Kuzmany, P. Ayala, M. Calvaresi, F. Zerbetto, T. Pichler, *Adv. Funct. Mater.* **2012**, *22*, 3202; b) P. Avouris, M. Freitag, V. Perebeinos, *Nat. Photonics* **2008**, *2*, 341; c) Y. Miyauchi, *J. Mater. Chem. C* **2013**, *1*, 6499.
[26] J. L. Wilbur, A. Kumar, E. Kim, G. M. Whitesides, *Adv. Mater.* **1994**, *6*, 600.
[27] a) K. Salaita, Y. Wang, C. A. Mirkin, *Nat. Nanotechnol.* **2007**, *2*, 145; b) F. Huo, Z. Zheng, G. Zheng, L. R. Giam, H. Zhang, C. A. Mirkin, *Science* **2008**, *321*, 1658; c) Z. Huang, L. Li, X. A. Zhang, N. Alsharif, X. Wu, Z. Peng, X. Cheng, P. Wang, K. A. Brown, Y. Wang, *Adv. Mater.* **2018**, *30*, 1705303.
[28] F. Huo, G. Zheng, X. Liao, L. R. Giam, J. Chai, X. Chen, W. Shim, C. A. Mirkin, *Nat. Nanotechnol.* **2010**, *5*, 637.
[29] X. Liao, K. A. Brown, A. L. Schmucker, G. L. Liu, S. He, W. Shim, C. A. Mirkin, *Nat. Commun.* **2013**, *4*, 2103.
[30] a) C. Carbonell, D. J. Valles, A. M. Wong, M. W. Tsui, M. Niang, A. B. Braunschweig, *Chem* **2018**, *4*, 857; b) X. M. Liu, Y. T. Zheng, S. R. Peurifoy, E. A. Kothari, A. B. Braunschweig, *Polym. Chem.* **2016**, *7*, 3229.
[31] H. Wilson, S. Ripp, L. Prisbrey, M. A. Brown, T. Sharf, D. J. T. Myles, K. G. Blank, E. D. Minot, *J. Phys. Chem. C* **2016**, *120*, 1971.
[32] D. Voiry, A. Goswami, R. Kappera, C. D. C. E. Silva, D. Kaplan, T. Fujita, M. W. Chen, T. Asefa, M. Chhowalla, *Nat. Chem.* **2015**, *7*, 45.
[33] P. Wang, Z. W. Peng, M. X. Li, Y. H. Wang, *Small* **2018**, *14*, 1802625.
[34] H. P. Liu, D. Nishide, T. Tanaka, H. Kataura, *Nat. Commun.* **2011**, *2*, 309.
[35] A. L. Ng, Y. Sun, L. Powell, C. F. Sun, C. F. Chen, C. S. Lee, Y. H. Wang, *Small* **2015**, *11*, 96.
[36] Z. Ming, B. A. Diner, *J. Am. Chem. Soc.* **2004**, *126*, 15490.
[37] Z. C. Wu, Z. H. Chen, X. Du, J. M. Logan, J. Sippel, M. Nikolou, K. Kamaras, J. R. Reynolds, D. B. Tanner, A. F. Hebard, A. G. Rinzler, *Science* **2004**, *305*, 1273.

 © 2020 WILEY-VCH Verlag GmbH & Co. KGaA, Weinheim